[aspartate aminotransferase], log [alanine aminotransferase], log [gamma-glutamyltransferase] and smoking habit, depending on application. Diabetes category was excluded for the analysis of diabetes, systolic blood pressure and diastolic blood pressure for the analysis of hypertension, and low-density lipoprotein cholesterol and log [high-density lipoprotein cholesterol] for the analysis of dyslipidemia.

doi:10.1371/journal.pone.0128972.g003

imbalances between cases and controls were less than 20% [23]. Table 6 shows the results of conditional logistic regression analysis for these case-matched subgroups. Results indicate that compared with WC and BMI, ABSI had weaker predictive power for the incidence of all three diseases.

Discussion

Our retrospective cohort study revealed that compared with BMI and WC, ABSI was not a better predictor of diabetes, hypertension, or dyslipidemia incidence in Japanese adults. In addition, using propensity score matching as an alternative evaluation method, the predictive power of ABSI for all three diseases was also lower than those of BMI and WC.

In American Caucasians, high ABSI accounted for a greater proportion of the total mortality hazard than did elevated BMI [13]. There are two possible reasons for this discrepancy. One is the different outcome measures used: all-cause mortality versus specific disease conditions. The other is racial differences. In regard to the first reason, a U-shaped or J-shaped association between all-cause mortality and BMI has been reported [1, 10, 13], while the associations of diabetes, hypertension, and dyslipidemia incidence [5] and prevalence [25, 26] with BMI are typically linear or nearly linear. In our study, near-linear associations between BMI and the incidence of diabetes and hypertension were also observed. In regard to the second reason, morphometric and physiological racial differences may alter the health implications of these indices. For example, the prevalence of obesity in Japanese adults was much lower than Americans [27]. In addition, East Asians, including the Japanese, are known to have limited innate capacity for insulin secretion, resulting in greater susceptibility to type 2 diabetes than Caucasians [28]. A prospective cohort study of Chinese adults of a smaller scale (n = 687) with the incidence of diabetes as the primary outcome has reported that the predictive power of ABSI was no better than that of WC or BMI [18]. In another study, the association of ABSI with hypertension incidence was found to be weaker than WC or BMI among 8,255 Indonesians [19]. Our results were consistent with those of these two studies of Asian subjects that examined the incidence of diabetes or hypertension as outcomes, even though the precise reasons for the discrepancy were unable to be ascertained. It should be noted that correlations between BMI, WC, and ABSI in our study were similar to those of Krakauer et al [13]. In brief, both studies found a high correlation between BMI and WC, a moderate correlation between ABSI and WC, but almost no correlation between ABSI and BMI.

ABSI was significantly associated with the incidence of diabetes and dyslipidemia even after adjustment for BMI. These BMI-independent associations may reflect the fact that ABSI represents central body mass, such as higher visceral fat accumulation, higher trunk fat accumulation, and lesser limb lean mass. Furthermore, in the sex- and age-adjusted models, the finding that the predictive power of ABSI for diabetes independent of BMI was significantly greater than that of WC, could be interesting (Table 2). If this is true, ABSI has an advantage over WC in predicting diabetes. However, this association was not observed in the multivariable-adjusted models (Table 3), after propensity score matching (Table 6), or in sensitivity analyses (Table 4). Thus, the stronger predictive power of ABSI might be confounded by other co-varying baseline characteristics.

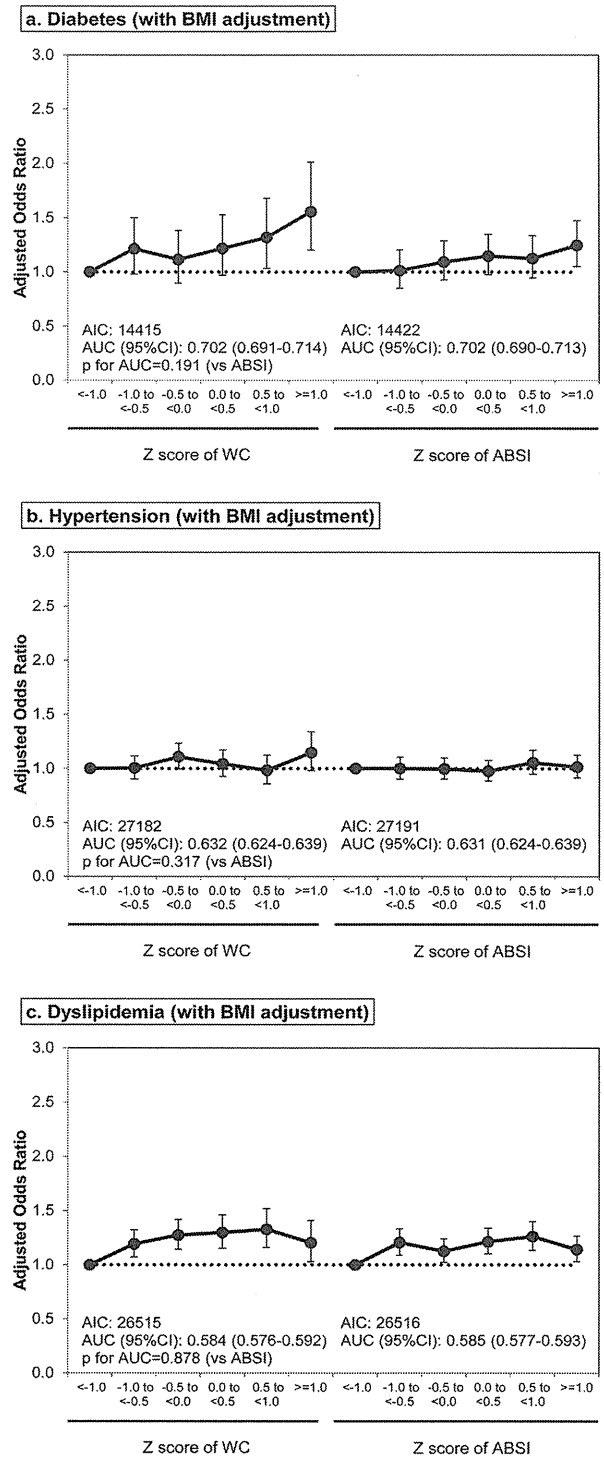

Fig 4. Odds ratio and 95% confidence interval of WC and ABSI categories for development of diabetes, hypertension and dyslipidemia with BMI adjustment. Abbreviations: BMI, body mass index; WC, waist circumference; ABSI, a body shape index; AIC, Akaike's information criterion; AUC, area under the curve; 95% CI, 95% confidence interval. Adjusted for BMI category in addition to same variables as shown in Fig 3.

doi:10.1371/journal.pone.0128972.g004

Table 4. Sensitivity analysis in subgroups stratified by sex.

	Men					Women					
	OR (95% CI)	p-value for OR	AIC	AUC (95% CI)	p-value for AUC[1]	OR (95% CI)	p-value for OR	AIC	AUC (95% CI)	p-value for AUC[1]	p-value for interaction[2]
Diabetes											
Without BMI adjustment[3]											
BMI	1.12 (1.04 –1.21)	0.002	7057	0.6385 (0.6212 –0.6557)	0.999	1.39 (1.30 –1.48)	<0.001	7350	0.7039 (0.6872 –0.7206)	<0.001	<0.001
WC	1.11 (1.03 –1.20)	0.005	7059	0.6384 (0.6211 –0.6556)	0.829	1.39 (1.29 –1.49)	<0.001	7358	0.7016 (0.6848 –0.7183)	<0.001	<0.001
ABSI	1.05 (0.98 –1.12)	0.132	7065	0.6369 (0.6197 –0.6542)	reference	1.08 (1.01 –1.15)	0.032	7437	0.6891 (0.6724 –0.7057)	reference	0.465
With BMI adjustment[4]											
WC	1.04 (0.92 –1.17)	0.566	7059	0.6386 (0.6213 –0.6556)	0.227	1.17 (1.06 –1.30)	0.002	7343	0.7048 (0.6881 –0.7215)	0.789	<0.001
ABSI	1.07 (0.99 –1.14)	0.053	7056	0.6396 (0.6224 –0.6569)	reference	1.11 (1.04 –1.19)	0.003	7343	0.7049 (0.6882 –0.7216)	reference	0.607
Hypertension											
Without BMI adjustment[3]											
BMI	1.26 (1.19 –1.34)	<0.001	9632	0.6157 (0.6028 –0.6287)	0.001	1.36 (1.30 –1.43)	<0.001	17487	0.6355 (0.6260 –0.6450)	<0.001	0.061
WC	1.20 (1.13 –1.27)	<0.001	9654	0.6116 (0.5986 –0.6246)	0.016	1.23 (1.18 –1.29)	<0.001	17574	0.6254 (0.6159 –0.6350)	<0.001	0.422
ABSI	1.00 (0.95 –1.05)	0.978	9693	0.6039 (0.5909 –0.6170)	reference	0.99 (0.96 –1.03)	0.619	17674	0.6157 (0.6062 –0.6253)	reference	0.637
With BMI adjustment[4]											
WC	1.01 (0.92 –1.10)	0.903	9634	0.6157 (0.6028 –0.6287)	0.665	1.01 (0.95 –1.07)	0.817	17489	0.6354 (0.6259 –0.6449)	0.395	0.166
ABSI	1.02 (0.97 –1.07)	0.418	9633	0.6159 (0.6029 –0.6288)	reference	1.00 (0.97 –1.04)	0.809	17489	0.6354 (0.5259 –0.6449)	reference	0.373
Dyslipidemia											
Without BMI adjustment[3]											
BMI	1.19 (1.13 –1.24)	<0.001	11208	0.5748 (0.5623 –0.5873)	0.004	1.14 (1.09 –1.19)	<0.001	15317	0.5775 (0.5670 –0.5880)	0.002	0.105
WC	1.17 (1.12 –1.23)	<0.001	11213	0.5735 (0.5611 –0.5860)	0.001	1.14 (1.10 –1.19)	<0.001	15314	0.5783 (0.5678 –0.5888)	<0.001	0.222

(*Continued*)

Table 4. (*Continued*)

	Men					Women					
	OR (95% CI)	p-value for OR	AIC	AUC (95% CI)	p-value for AUC[1]	OR (95% CI)	p-value for OR	AIC	AUC (95% CI)	p-value for AUC[1]	p-value for interaction[2]
ABSI	1.04 (0.99 –1.08)	0.115	11252	0.5621 (0.5495 –0.8747)	reference	1.04 (1.00 –1.79)	0.040	15351	0.5688 (0.5582 –0.5793)	reference	0.965
With BMI adjustment[4]											
WC	1.07 (0.99 –1.16)	0.117	11208	0.5755 (0.5630 –0.5879)	0.171	1.09 (1.03 –1.16)	0.006	15312	0.5794 (0.5689 –0.5899)	0.186	0.290
ABSI	1.05 (1.00 –1.99)	0.030	11205	0.5762 (0.5637 –0.5886)	reference	1.05 (1.01 –1.08)	0.020	15314	0.5790 (0.5685 –0.5895)	reference	0.821

OR, odds ratio; CI, confidence interval; ABSI, a body shape index; WC, waist circumference; BMI, body mass index; AIC, Akaike's information criterion; AUC, area under the curve

Subjects were 13,588 men and 23,993 women without diabetes at baseline, 7,685 men and 15,405 women without hypertension at baseline, and 8,958 men and 11,818 women without dyslipidemia at baseline.

[1] p-value with Bonferroni's correction

[2] p-value for interaction of sex with BMI, WC, and ABSI

[3]Adjusted for baseline characteristics, including age (continuous variable, year), diabetes category, systolic blood pressure, diastolic blood pressure, low-density lipoprotein cholesterol, log [high-density lipoprotein cholesterol], log [aspartate aminotransferase], log [alanine aminotransferase], log [gamma-glutamyltransferase] and smoking habit, except for diabetes category in the analysis of diabetes, systolic blood pressure and diastolic blood pressure in the analysis of hypertension, and low-density lipoprotein cholesterol and log [high-density lipoprotein cholesterol] in the analysis of dyslipidemia.

[4]Adjusted for BMI Z-score and the variables described above

doi:10.1371/journal.pone.0128972.t004

We found that the predictive powers of BMI and WC for diabetes incidence are greater in women than in men, while that of ABSI does not differ by sex (Table 4). Cross-sectional studies in the Japanese population [29] and in the Framingham Heart Study [30] have shown that associations of metabolic risk factors, such as systolic and diastolic blood pressure, fasting glucose, and total cholesterol, with increasing volumes both of subcutaneous and visceral fat, strictly measured by computed tomography, were stronger in women than in men. Our observation of a sex difference in BMI and WC could be the same phenomenon, but this is not the case with ABSI. Thus, ABSI might have an implication for disease incidence that is different from BMI or WC. Further studies are necessary to conclude whether this difference is true or not.

The following four limitations in our study are conceivable. First, due to the retrospective cohort design, we could not obtain other potentially relevant data, such as alcohol consumption and levels of physical activity, which may confound the associations of BMI, WC, and ABSI with disease incidence. To correct this, we have made adjustment for potential confounding factors as much as possible using logistic regression analysis and the propensity score matching method. Second, fasting blood glucose data for some subjects were not available. To compensate for this, we employed HbA1c data and history of diabetes medication to obtain an accurate diagnosis. Third, some bias might exist that resulted in underestimation of associations because the reasons and outcomes of non-attendance of annual health checkup are unknown. Fourth, the generalizability of our findings might be limited because the subjects are

Table 5. Baseline characteristics of controls and cases after propensity score matching.

	Diabetes				Hypertension				Dyslipidemia			
	Without Incidence (controls)	With Incidence (cases)	p-value	SD (%)	Without Incidence (controls)	With Incidence (cases)	p-value	SD (%)	Without Incidence (controls)	With Incidence (cases)	p-value	SD (%)
Number of subjects	1,947	1,947			6,962	6,962			7,263	7,263		
Men percent [a]	53.6	52.6	0.477	1.4[c]	38.0	38.3	0.220	-0.4[c]	40.4	40.4	0.971	0.0[c]
Age (years)[b]	64.4 (5.6)	64.5 (5.4)	0.526	2.0[c]	63.9 (5.7)	63.9 (5.8)	0.382	0.9[c]	63.3 (6.8)	63.3 (6.5)	0.726	0.5[c]
BMI	23.5 (3.2)	24.1 (3.4)	<0.001	-19.3	22.1 (2.8)	22.7 (2.9)	<0.001	-20.2	22.3 (3.1)	22.7 (3.1)	<0.001	-12.3
WC	84.4 (8.5)	85.9 (9.0)	<0.001	-17.1	80.8 (8.5)	82.2 (8.6)	<0.001	-15.6	80.9 (9.0)	82.1 (8.8)	<0.001	-13.2
ABSI	0.0817 (0.0048)	0.0818 (0.0048)	0.217	-4.0	0.0816 (0.0053)	0.0816 (0.0052)	0.713	0.6	0.0812 (0.0052)	0.0815 (0.0051)	0.002	-5.0
Diabetes category [a]												
Normal	89.3	43.5	<0.001	90.5	83.4	83.1	0.817	0.8[c]	83.2	83.3	0.235	-0.2[c]
Borderline	10.7	56.6		-64.4	9.3	9.3		-0.1[c]	9.0	9.3		-0.2[c]
Diabetes	-	-			7.4	7.6		-0.3[c]	7.7	7.4		0.3[c]
SBP (mmHg)	134 (17)	133 (16)	0.490	2.1[c]	118 (11)	126 (9)	<0.001	-78.2	129 (17)	129 (17)	0.958	-0.1[c]
DBP (mmHg)	79 (11)	79 (10)	0.983	-0.1[c]	71 (8)	76 (8)	<0.001	-56.6	77 (11)	77 (11)	0.944	0.1[c]
LDL-C (mg/dl)	128 (32)	128 (32)	0.664	1.4[c]	129 (31)	129 (31)	0.498	1.1[c]	107 (19)	122 (15)	<0.001	-88.0
Log HDL-C	4.06 (0.26)	4.06 (0.26)	0.988	0.0[c]	4.14 (0.26)	4.14 (0.27)	0.545	0.9[c]	4.21 (0.24)	4.12 (0.25)	<0.001	36.5
Log AST	3.18 (0.34)	3.19 (0.35)	0.307	-3.0[c]	3.13 (0.29)	3.13 (0.30)	0.788	-0.4[c]	3.12 (0.30)	3.12 (0.30)	0.463	1.2[c]
Log ALT	3.14 (0.48)	3.15 (0.50)	0.357	-2.3[c]	2.97 (0.44)	2.98 (0.45)	0.756	-0.5[c]	2.95 (0.43)	2.95 (0.45)	0.721	0.6[c]
Log GGT	3.55 (0.72)	3.54 (0.71)	0.936	0.2[c]	3.27 (0.63)	3.28 (0.65)	0.503	-0.9[c]	3.28 (0.69)	3.28 (0.68)	0.868	0.3[c]
Smoking habit [a]	19.0	19.3	0.798	-0.3[c]	14.0	13.9	0.843	0.1[c]	14.0	13.7	0.701	0.2[c]

SD, standardized difference; SBP, systolic blood pressure; DBP, diastolic blood pressure; LDL-C, low-density lipoprotein cholesterol; HDL-C, high-density lipoprotein cholesterol; AST, aspartate aminotransferase; ALT, alanine aminotransferase; GGT, gamma-glutamyltransferase

[a] Percentage and p-value by McNemar's test

[b] Mean (standard deviation) and p-value by paired t-test

[c] These variables were used for calculating the propensity score

doi:10.1371/journal.pone.0128972.t005

mainly elderly adults living in one urban area of Japan with a relatively higher incidence of hypertension (30.2%) and dyslipidemia (35.0%) during the 4-year period. On the other hand, the major advantage of our study is that we obtained consistent results using two different covariate adjustment methods (logistic regression analysis and the propensity score matching) and also from sensitivity analyses. Furthermore, new-onset diabetes, hypertension, and dyslipidemia was confirmed both by self-reported medication use and physiological measures. Since subjects are not always aware of their disease, we may underestimate disease incidence when it is determined only by self-reported medication use.

In conclusion, ABSI was not a better predictor of diabetes, hypertension, and dyslipidemia incidence than BMI and WC in Japanese adults. However, ABSI had significant associations with the incidence of diabetes and dyslipidemia independently of BMI.

Table 6. Associations between disease incidence (diabetes, hypertension, and dyslipidemia) and Z-scores for BMI, WC, and ABSI as revealed by conditional logistic regression analysis of case-matched subsets obtained by propensity score matching.

	OR (95% CI)	p-value for OR	AIC	AUC (95% CI)	p-value for AUC[1]
Diabetes					
Without BMI adjustment					
BMI	1.20 (1.13–1.28)	<0.001	2666	0.5549 (0.5369–0.5729)	0.002
WC	1.18 (1.11–1.26)	<0.001	2676	0.5456 (0.5275–0.5636)	<0.001
ABSI	1.03 (0.96–1.10)	0.385	2700	0.5098 (0.4917–0.5280)	reference
With BMI adjustment[2]					
WC	1.02 (0.91–1.15)	0.680	2668	0.5546 (0.5366–0.5726)	0.682
ABSI	1.05 (0.98–1.12)	0.134	2666	0.5554 (0.5374–0.5734)	reference
Hypertension					
Without BMI adjustment					
BMI	1.26 (1.21–1.31)	<0.001	9512	0.5567 (0.5472–0.5662)	<0.001
WC	1.18 (1.14–1.23)	<0.001	9570	0.5419 (0.5323–0.5514)	<0.001
ABSI	0.99 (0.96–1.03)	0.713	9653	0.5025 (0.4929–0.5121)	reference
With BMI adjustment[2]					
WC	0.99 (0.94–1.05)	0.830	9514	0.5567 (0.5472–0.5663)	0.500
ABSI	1.00 (0.97–1.03)	0.995	9514	0.5567 (0.5472–0.5662)	reference
Dyslipidemia					
Without BMI adjustment					
BMI	1.14 (1.10–1.18)	<0.001	10015	0.5386 (0.5293–0.5480)	0.001
WC	1.15 (1.11–1.19)	<0.001	10006	0.5391 (0.5298–0.5485)	<0.001
ABSI	1.05 (1.02–1.09)	0.003	10062	0.5150 (0.5056–0.5244)	reference
With BMI adjustment[2]					
WC	1.11 (1.04–1.17)	0.001	10005	0.5409 (0.5315–0.5503)	0.600
ABSI	1.06 (1.02–1.09)	0.001	10006	0.5412 (0.5318–0.5506)	reference

OR, odds ratio; CI, confidence interval; ABSI, a body shape index; WC, waist circumference; BMI, body mass index; AIC, Akaike's information criterion; AUC, area under the curve

[1] p-value with Bonferroni's correction

[2] Adjusted for BMI

doi:10.1371/journal.pone.0128972.t006

Supporting Information

S1 Table. Baseline characteristics of retained subjects and dropouts during follow-up.
(DOCX)

Acknowledgments

This study was supported by a grant for MEXT KAKENHI Grant Number 26460826, Joint Research Projects between Chiba City and Universities, 2013, and Grants from Chiba Foundation Health Promotion & Disease Prevention.

We greatly appreciate the invaluable help and support from staff of Chiba City Hall, Toshie Kakinuma, Yoshio Sato, Takayo Horinoguchi, Takao Imazeki, Takehumi Fujiyama, and Takehumi Kajiwara, who provided all data analyzed in this study.

Author Contributions

Conceived and designed the experiments: MF YS KN. Performed the experiments: MF AH. Analyzed the data: MF. Contributed reagents/materials/analysis tools: YS KN ST. Wrote the paper: MF YS KN ST AH. Data acquisition: MF AH. Data interpretation: YS KN ST. Supervision or mentorship: AH.

References

1. Berrington de Gonzalez A, Hartge P, Cerhan JR, Flint AJ, Hannan L, MacInnis RJ, et al. (2010) Body-mass index and mortality among 1.46 million white adults. N Engl J Med 363: 2211–2219. doi: 10.1056/NEJMoa1000367 PMID: 21121834
2. Flegal KM, Kit BK, Orpana H, Graubard BI (2013) Association of all-cause mortality with overweight and obesity using standard body mass index categories: a systematic review and meta-analysis. JAMA 309: 71–82. doi: 10.1001/jama.2012.113905 PMID: 23280227
3. Jiang J, Ahn J, Huang WY, Hayes RB (2013) Association of obesity with cardiovascular disease mortality in the PLCO trial. Prev Med 57: 60–64. doi: 10.1016/j.ypmed.2013.04.014 PMID: 23632233
4. Fujita M, Ueno K, Hata A (2009) Effect of obesity on incidence of type 2 diabetes declines with age among Japanese women. Exp Biol Med 234: 750–757. doi: 10.3181/0810-RM-292 PMID: 19429850
5. Ishikawa-Takata K, Ohta T, Moritaki K, Gotou T, Inoue S (2002) Obesity, weight change and risks for hypertension, diabetes and hypercholesterolemia in Japanese men. Eur J Clin Nutr 56: 601–607. PMID: 12080398
6. Pereira M, Lunet N, Paulo C, Severo M, Azevedo A, Barros H (2012) Incidence of hypertension in a prospective cohort study of adults from Porto, Portugal. BMC Cardiovasc Disord 12: 114. doi: 10.1186/1471-2261-12-114 PMID: 23190867
7. Nevill AM, Stewart AD, Olds T, Holder R (2006) Relationship between adiposity and body size reveals limitations of BMI. Am J Phys Anthropol 129: 151–156. PMID: 16270304
8. Gómez-Ambrosi J, Silva C, Galofré JC, Escalada J, Santos S, Millán D, et al. (2012) Body mass index classification misses subjects with increased cardiometabolic risk factors related to elevated adiposity. Int J Obes 36: 286–294. doi: 10.1038/ijo.2011.100 PMID: 21587201
9. Ruhl CE, Everhart JE (2010) Trunk fat is associated with increased serum levels of alanine aminotransferase in the United States. Gastroenterology 138: 1346–1356. doi: 10.1053/j.gastro.2009.12.053 PMID: 20060831
10. Czernichow S, Kengne AP, Stamatakis E, Hamer M, Batty GD (2011) Body mass index, waist circumference and waist-hip ratio: which is the better discriminator of cardiovascular disease mortality risk?: evidence from an individual-participant meta-analysis of 82 864 participants from nine cohort studies. Obes Rev 12: 680–687. doi: 10.1111/j.1467-789X.2011.00879.x PMID: 21521449
11. Welborn TA, Dhaliwal SS (2007) Preferred clinical measures of central obesity for predicting mortality. Eur J Clin Nutr 61: 1373–1379. PMID: 17299478
12. Moore SC (2009) Waist versus weight: which matters more for mortality? Am J Clin Nutr 89: 1003–1004. doi: 10.3945/ajcn.2009.27598 PMID: 19244373
13. Krakauer NY, Krakauer JC (2012) A new body shape index predicts mortality hazard independently of body mass index. PLoS One 7: e39504. doi: 10.1371/journal.pone.0039504 PMID: 22815707
14. Song X, Jousilahti P, Stehouwer CD, Söderberg S, Onat A, Laatikainen T, et al. (2013) Comparison of various surrogate obesity indicators as predictors of cardiovascular mortality in four European populations. Eur J Clin Nutr 23: 1298–1302.
15. Krakauer NY, Krakauer JC (2014) Dynamic association of mortality hazard with body shape. PLoS One. 9: e88793. doi: 10.1371/journal.pone.0088793 PMID: 24586394
16. Afsar B, Elsurer R, Kirkpantur A (2013) Body shape index and mortality in hemodialysis patients. Nutrition 29: 1214–1218. doi: 10.1016/j.nut.2013.03.012 PMID: 23830741
17. Abete I, Arriola L, Etxezarreta N, Mozo I, Moreno-Iribas C, Amiano P, et al. (2014) Association between different obesity measures and the risk of stroke in the EPIC Spanish cohort. Eur J Nutr. in press. Available: http://link.springer.com/article/10.1007%2Fs00394-014-0716-x. Accessed 27 August 2014.
18. He S, Chen X (2013) Could the new body shape index predict the new onset of diabetes mellitus in the Chinese population? PLoS One 8: e50573. doi: 10.1371/journal.pone.0050573 PMID: 23382801
19. Cheung YB (2014) "A Body Shape Index" in middle-age and older Indonesian population: scaling exponents and association with incident hypertension. PLoS One 9: e85421. doi: 10.1371/journal.pone.0085421 PMID: 24454862

20. Seino Y, Nanjo K, Tajima N, Kadowaki T, Kashiwagi A, Araki E, et al. The Committee of the Japan Diabetes Society on the diagnostic criteria of diabetes mellitus. (2010) Report of the Committee on the classification and diagnostic criteria of diabetes mellitus. Diabetol Int 1: 2–20.

21. The Japanese Society of Hypertension (2009) Guideline for the management of hypertension 2009 (Japanese). Tokyo: Life Science Publishing Co., Ltd.

22. Committee for Epidemiology and Clinical Management of Atherosclerosis (2013) Executive summary of the Japan Atherosclerosis Society (JAS) guidelines for the diagnosis and prevention of atherosclerotic cardiovascular diseases in Japan -2012 version. J Atheroscler Thromb 20: 517–523. PMID: 23665881

23. Dongsheng Y, Jarrod ED. A unified approach to measuring the effect size between two groups using SAS. Available: http://support.sas.com/resources/papers/proceedings12/335-2012.pdf#search=%27aunified+approach+to+measuring+effect+size+sas%27. Accessed 09 July 2014.

24. Parsons LS, Ovation Research Group. Reducing bias in a propensity score matches-pair sample using greedy matching techniques. Available: http://www2.sas.com/proceedings/sugi26/p214-26.pdf#search=%27reducing+bias+in+propensity+score+matched+pair+greedy+matching%27. Accessed 09 July 2014.

25. Bays HE, Chapman RH, Grandy S; SHIELD Investigators' Group (2007) The relationship of body mass index to diabetes mellitus, hypertension and dyslipidaemia: comparison of data from two national surveys. Int J Clin Pract 61: 737–747. PMID: 17493087

26. Schmiegelow MD, Andersson C, Køber L, Andersen SS, Norgaard ML, Jensen TB, et al. (2014) Associations between body mass index and development of metabolic disorders in fertile women—a nationwide cohort study. J Am Heart Assoc 10; doi: 10.1161/JAHA.113.000672

27. World Health Organization. World Health Statistics 2013. http://www.who.int/gho/publications/world_health_statistics/2013/en/. Accessed 3 April 2013

28. Kodama K, Tojjar D, Yamada S, Toda K, Patel CJ, Butte AJ (2013) Ethnic differences in the relationship between insulin sensitivity and insulin response: a systematic review and meta-analysis. Diabetes Care 36: 1789–1796. doi: 10.2337/dc12-1235 PMID: 23704681

29. Oka R, Miura K, Sakurai M, Nakamura K, Yagi K, Miyamoto S, et al. (2010) Impacts of visceral adipose tissue and subcutaneous adipose tissue on metabolic risk factors in middle-aged Japanese. Obesity 18:153–160. doi: 10.1038/oby.2009.180 PMID: 19498348

30. Fox CS, Massaro JM, Hoffmann U, Pou KM, Maurovich-Horvat P, Liu CY, et al. (2007) Abdominal visceral and subcutaneous adipose tissue compartments: association with metabolic risk factors in the Framingham Heart Study. Circulation 116: 39–48. PMID: 17576866

Hatakeyama *et al. Acta Neuropathologica Communications* (2015) 3:52
DOI 10.1186/s40478-015-0227-x

ACTA NEUROPATHOLOGICA COMMUNICATIONS

RESEARCH Open Access

Molecular pathomechanisms and cell-type-specific disease phenotypes of MELAS caused by mutant mitochondrial tRNA^{Trp}

Hideyuki Hatakeyama[1,2*], Ayako Katayama[3], Hirofumi Komaki[1,3], Ichizo Nishino[4,5] and Yu-ichi Goto[1,2,3,5*]

Abstract

Introduction: Numerous pathogenic mutations responsible for mitochondrial diseases have been identified in mitochondrial DNA (mtDNA)-encoded tRNA genes. In most cases, however, the detailed molecular pathomechanisms and cellular pathophysiology of these mtDNA mutations —how such genetic defects determine the variation and the severity of clinical symptoms in affected individuals— remain unclear. To investigate the molecular pathomechanisms and to realize *in vitro* recapitulation of mitochondrial diseases, intracellular mutant mtDNA proportions must always be considered.

Results: We found a disease-causative mutation, m.5541C>T heteroplasmy in *MT-TW* gene, in a patient exhibiting mitochondrial myopathy, encephalopathy, lactic acidosis, and stroke-like episodes (MELAS) with multiple organ involvement. We identified the intrinsic molecular pathomechanisms of m.5541C>T. This mutation firstly disturbed the translation machinery of mitochondrial tRNA^{Trp} and induced mitochondrial respiratory dysfunction, followed by severely injured mitochondrial homeostasis. We also demonstrated cell-type-specific disease phenotypes using patient-derived induced pluripotent stem cells (iPSCs) carrying ~100 % mutant m.5541C>T. Significant loss of terminally differentiated iPSC-derived neurons, but not their stem/progenitor cells, was detected most likely due to serious mitochondrial dysfunction triggered by m.5541C>T; in contrast, m.5541C>T did not apparently affect skeletal muscle development.

Conclusions: Our iPSC-based disease models would be widely available for understanding the "definite" genotype-phenotype relationship of affected tissues and organs in various mitochondrial diseases caused by heteroplasmic mtDNA mutations, as well as for further drug discovery applications.

Keywords: Mitochondrial myopathy, encephalopathy, lactic acidosis, stroke-like episodes (MELAS), Mutant mitochondrial tRNA^{Trp}, Mitochondrial respiratory dysfunction, Induced pluripotent stem cells (iPSCs), *in vitro* cellular disease models

* Correspondence: hideyuki@ncnp.go.jp; goto@ncnp.go.jp
[1]Department of Mental Retardation and Birth Defect Research, National Institute of Neuroscience, National Center of Neurology and Psychiatry, Kodaira, Tokyo 187-8502, Japan
Full list of author information is available at the end of the article

Introduction

Mitochondrial DNA (mtDNA) has unique translation and transcription machinery and is associated with the maintenance of cellular homeostasis through intergenomic crosstalk with nuclear DNA (nDNA). Numerous pathogenic mutations responsible for various mitochondrial diseases have been identified in mtDNA-encoded tRNA genes [1], and in most cases, such disease-causative heteroplasmic mutations (*i.e.*, wild-type mtDNA and mutant mtDNA co-exist within a cell) exhibit their intrinsic pathogenic thresholds. Mutant mitochondrial tRNAs frequently induce various loss-of-function at a molecular level [2] including not only damaged mitochondrial protein synthesis, but also inhibited aminoacylation [3], tRNA molecular instability [4], altered tRNA processing [5], wobble-base modification deficiency [6, 7], or a combination of these. Therefore, the degree of accumulated mutant mitochondrial tRNAs within a cell is most likely to determine the trajectory of tissue- and organ-specific disease progression and phenotypic severity in affected individuals. Focusing on *MT-TW* gene, which encodes mitochondrial $tRNA^{Trp}$, several pathogenic mutations have been reported to cause widespread clinical symptoms in relation to mitochondrial diseases (*e.g.*, encephalopathy, myopathy, dementia and chorea, gastrointestinal syndrome, or severe multiple organ disorders) [8–13].

Mitochondrial myopathy, encephalopathy, lactic acidosis, and stroke-like episodes (MELAS) is genetically heterogeneous and presents a broad clinical spectrum among individuals [14] including variations in age of onset (infantile to adolescence) or affected tissues and organs (central nervous system, cardiovascular system, neuromuscular system, endocrine system, gastrointestinal system, or a combination of these). Such variations may depend on the influence of molecular defects in mitochondrial respiratory chain complexes I and/or IV (CI and/or CIV) on mitochondrial energy metabolism and oxidative stress in various terminally differentiated cell types in affected individuals. To date, however, limited somatic cell types (*e.g.*, fibroblasts, myoblasts, or lymphoblasts) are available to characterize patient-specific pathophysiology of affected tissues and organs in mitochondrial diseases. Recently, the generation of induced pluripotent stem cells (iPSCs) from various human somatic cells by forced ectopic expression of several pluripotency-associated transcription factors has been reported [15, 16], and patient-derived iPSCs carrying mutant mtDNAs have therefore opened new avenues for facilitating mitochondrial medicine.

In this study, we found a disease-causative mutation, m.5541C > T heteroplasmy in *MT-TW* gene, in a patient exhibiting MELAS with multiple organ involvement. We identified the intrinsic molecular pathomechanisms of m.5541C > T and demonstrated cell-type-specific disease phenotypes using patient-derived iPSCs carrying ~100 % mutant m.5541C > T. Our iPSC-based disease models would be widely available for understanding the definitive genotype-phenotype relationship of affected tissues and organs in various mitochondrial diseases caused by heteroplasmic mtDNA mutations, as well as for further drug discovery applications.

Patients and methods

Patients

This study was approved by our Institutional Review Board and was stringently conducted in accordance with the ethical principles of the "Declaration of Helsinki". Patient biopsy was performed for diagnostic purposes only after we received written informed consent with permission to study patient-derived iPSCs. Note that 10 control subjects were also used in this study.

A partial family pedigree for this patient is shown (Fig. 1a). In this family, there was no clinical history of any neuromuscular disease. He had no growth and mental retardation until firstly presenting epileptic symptoms at age 10 years. At age 11 years, he developed weight loss, activity loss, easy fatigue, cognitive impairment, and acute heart failure. Radiographic and ultracardiographic images revealed hypertrophic cardiomyopathy at interventricular septum and left ventricular wall (Fig. 1b). Markedly increased serum lactate level (114.7 mg/dL; 3.0-17.0 mg/dL as normal), serum pyruvate level (3.86 mg/dL; 0.30–0.94 mg/dL as normal), and lactate/pyruvate ratio (29.7) were detected. At age 13 years, he developed headache, vomiting, visual disturbance, convulsion, and myoclonic status with unconsciousness. Brain MRI revealed multifocal hyper-intensity lesions at basal ganglia, cortex, and subcortical white matter of both cerebrum and cerebellum. A representative lesion showed decreased N-acetylaspartate level and increased lactate level (Fig. 1c). On this occasion, no significant abnormalities in serum lactate level (18.9 mg/dL), serum pyruvate level (0.99 mg/dL), or lactate/pyruvate ratio (19.0) were detected; however, cerebrospinal fluid lactate level (41.5 mg/dL), cerebrospinal fluid pyruvate level (1.40 mg/dL), and lactate/pyruvate ratio (29.6) were clearly high. Skeletal muscle histopathology revealed diffuse cytochrome *c* oxidase (COX) deficiency (less than 5 % population of COX-positive fibers) (Fig. 1d); however, no other typical pathological abnormalities such as ragged-red-fibers or strongly succinate dehydrogenase (SDH)-reactive blood vessels were observed. We diagnosed this patient as MELAS and started oral administration of l-arginine, dichloroacetate, and sodium pyruvate. He relapsed with stroke-like episodes twice in 4 years. At age 14 years, he developed multiple organ involvement

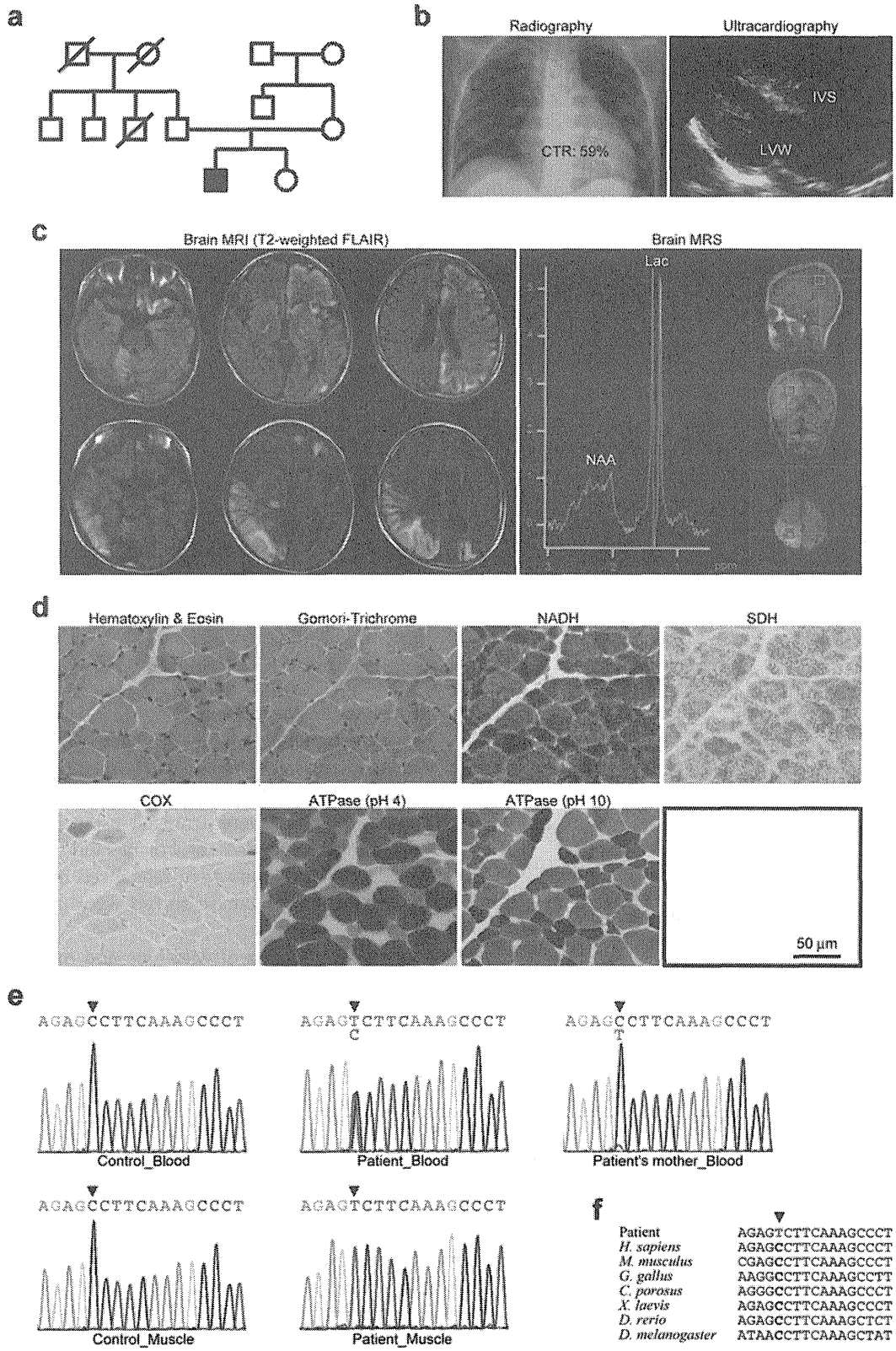

Fig. 1 (See legend on next page.)

(See figure on previous page.)
Fig. 1 Clinical diagnosis and molecular genetic analysis for the patient. **a** A partial family pedigree. Filled square indicates this patient. **b** Radiographic and ultracardiographic images for this patient at age 11 years, indicating hypertrophic cardiomyopathy. Cardiothoracic ratio (CTR) in radiographic image is also shown. **c** T2-weighted FLAIR images of brain MRI for this patient at age 13 years, indicating multifocal stroke-like episodes. Brain MRS also shows decreased N-acetylaspartate (NAA) level and increased lactate (Lac) level. **d** Histopathology against serial frozen sections of biopsied skeletal muscle specimens from this patient at age 13 years, indicating diffuse COX deficiency. **e** Electropherograms of the anticodon domain of *MT-TW* gene for extracted DNA from blood tissues and skeletal muscle tissues of both control and this patient. Arrowheads indicate m.5541C > T. Note that the same mutation was also found in blood tissues from this patient's asymptomatic mother. **f** Alignment of sequences in the anticodon-stem and the anticodon-loop of *MT-TW* gene from various eukaryotes. Arrowhead indicates m.5541C > T. Blue-colored characters indicate the anticodon recognition site of mitochondrial $tRNA^{Trp}$

including acute pancreatitis, gastrointestinal malabsorption, renal tubular disturbance, and endocrine glucose intolerance. At age 15 years, he developed quadriparesis. Now, he keeps stable condition without serious trouble.

Myoblast culture

Patient-derived skeletal muscle tissues were minced, enzymatically digested, and centrifuged to collect myoblasts according to standard protocol. Patient-derived myoblasts were maintained in DMEM/F12 (Gibco) supplemented with 20 % FBS (Gibco), 100 units/mL penicillin (Gibco), 100 μg/mL streptomycin (Gibco) at 37 °C under humidified atmosphere of 5 % CO_2. During establishment of patient-derived primary myoblasts, 0.5 μg/mL MC210 (DS Pharm) as a mycoplasmacidal reagent and 2.5 μg/mL fungizone (Gibco) as a fungicidal reagent were also added to culture medium.

Terminal differentiation of patient-derived myoblasts into myotubes was performed as follows: Briefly, patient-derived myoblasts were seeded at high cell density onto 6-well culture plates and were maintained at 37 °C under humidified atmosphere of 5 % CO_2. After 3 days in culture, culture medium was switched to myogenic differentiation medium (Cell Applications) supplemented with 100 units/mL penicillin (Gibco), 100 μg/mL streptomycin (Gibco), and patient-derived myoblasts were maintained at 37 °C under humidified atmosphere of 5 % CO_2 for 2 weeks.

Analysis of mtDNA mutation

Long PCR-based whole mtDNA sequencing for the patient was performed as described elsewhere [17] with modifications to eliminate any adverse results arising from pseudo-sequences in nuclear DNA: Briefly, extracted DNA as template (10 ng for iPSCs, 20 ng for myoblasts and skeletal muscle tissues, 100 ng for blood tissues) was amplified via mtDNA-specific long-range PCR and the following mtDNA-specific nested PCR with a thermal cycler (GeneAmp PCR System 9700; Applied Biosystems). The amplified mtDNA fragments were sequenced with a DNA analyzer (ABI PRISM 3130xl; Applied Biosystems). The obtained mtDNA sequence data from each patient was compared with the databases of "Human Mitochondrial Genome Database (MITOMAP; http://www.mitomap.org/MITOMAP/)" and "Human Mitochondrial Genome Polymorphism (mtSNP; http://mtsnp.tmig.or.jp/mtsnp/)" [18] to find any genetic variants.

Mutation ratio of m.5541C > T in the patient was determined as follows: Extracted DNA (1 ng) was used as template for quantitative PCR with TaqMan Universal PCR Master Mix kit (Applied Biosystems) according to the manufacturer's instructions. A sequence detection system (ABI PRISM 7900HT; Applied Biosystems) was used, and a calibration curve was created using several copy-number standards with plasmids containing the amplified mtDNA fragments (nucleotide position in mtDNA; 5205–5767) for either wild-type or mutant sequences.

Protein and tRNA modeling

in silico modeling of bovine heart CIV homodimer in fully oxidized state [19] was performed on the database of "RCSB Protein Data Bank (http://www.rcsb.org/pdb/)", and the graphics were arranged using RasMol software. Amino acid sequences of bovine and human mtDNA-encoded CIV subunits were referenced in the database of "NCBI Protein Database (http://www.ncbi.nlm.nih.gov/protein/)".

in silico modeling of wild-type and mutant mitochondrial $tRNA^{Trp}$ were performed on the database of "Vienna RNA Servers (http://rna.tbi.univie.ac.at/)", and representative physicochemical parameters (*e.g.*, minimum free energy and base-pair probability) were simultaneously calculated.

Reverse transcription PCR (RT-PCR) and quantitative PCR

Reverse transcription was performed with PrimeScript RT Master Mix kit (TaKaRa Bio) according to the manufacturer's instructions. After reverse transcription of extracted total RNA, total cDNA (25 ng) was used as template for RT-PCR with a thermal cycler (GeneAmp PCR system 9700; Applied Biosystems). The amplified PCR products were resolved via electrophoresis through 2 % agarose gel, stained with GelGreen (Biotium), and detected with a UV transilluminator (GelDoc-It Imaging System; UVP).

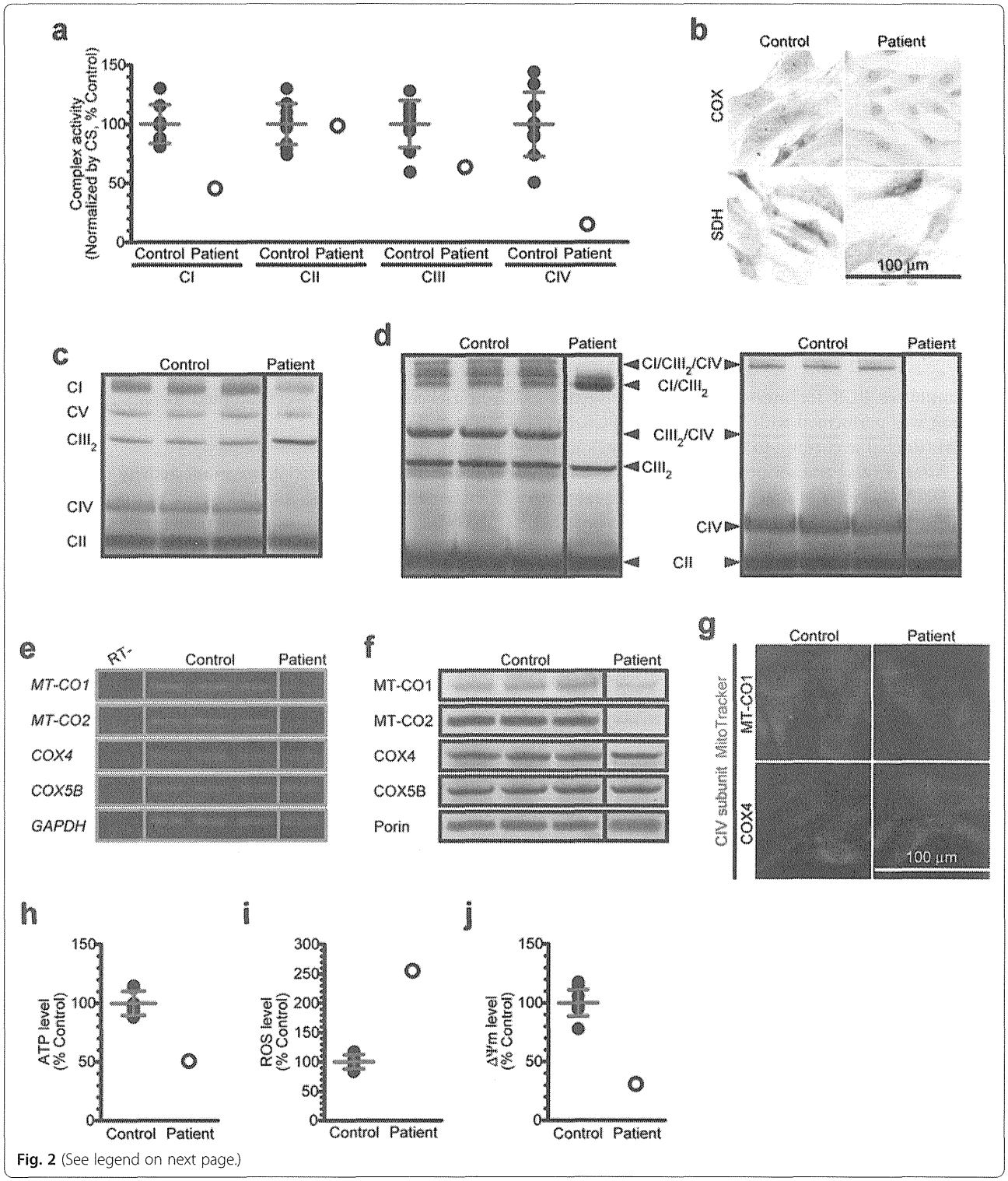

Fig. 2 (See legend on next page.)

(See figure on previous page.)
Fig. 2 Mutant mitochondrial $tRNA^{Trp}$ triggers widespread mitochondrial dysfunction. **a** Enzymatic activities of individual mitochondrial respiratory chain complexes for cultured myoblasts of both controls (n = 10, closed circles) and the patient (open circles). Error bars indicate as the means with SD of controls. All samples were measured in triplicate and averaged. **b** Representative images of cytochemical staining of COX and SDH for cultured myoblasts from both controls and the patient. Cell nuclei were co-stained with hematoxylin. **c,d** Immunodetection of **c** individual respiratory chain complexes and **d** respiratory chain supercomplexes for isolated mitochondria from cultured myoblasts of both controls and the patient. **e** Gene expression of several CIV structural subunits for extracted mRNA from cultured myoblasts of both controls and the patient. **f** Protein expression of several CIV structural subunits for isolated mitochondria from cultured myoblasts of both controls and the patient. **g** Representative images of immunocytochemical staining of CIV structural subunits for cultured myoblasts of both controls and the patient; MT-CO1 (red), COX4 (red). Mitochondria were co-stained with MitoTracker (green). **h** ATP level for cultured myoblasts of both controls (n = 10, closed circles) and the patient (open circles). Error bar indicates as the mean with SD of controls. All samples were measured in triplicate and averaged. **i** Oxidative stress level for cultured myoblasts of both controls (n = 10, closed circles) and the patient (open circle). Fluorescence intensity ratio of MitoSOX/MitoTracker served as mitochondrial ROS level. Error bar indicates as the mean with SD of controls. All samples were measured in triplicate and averaged. **j** Membrane potential ($\Delta\Psi m$) level for cultured myoblasts of both controls (n = 10, closed circles) and the patient (open circle). Fluorescence intensity ratio of JC-1 dye aggregates/monomers served as mitochondrial $\Delta\Psi m$ level. Error bar indicates as the mean with SD of controls. All samples were measured in triplicate and averaged

Quantitative PCR for measurement of transgenes expression was performed with SYBR Green I PCR Master Mix kit (Roche) according to the manufacturer's instructions. After reverse transcription of extracted total RNA, total cDNA (10 ng) was used as template for quantitative PCR with a real-time PCR system (LightCycler 480II; Roche). The averaged threshold cycle number for housekeeping genes were adopted for $\Delta\Delta C_T$-based relative quantification.

Analysis of mitochondrial enzymatic activity

Enzymatic activities for individual mitochondrial respiratory chain complexes were analyzed as described elsewhere [20] with modifications: Cultured and

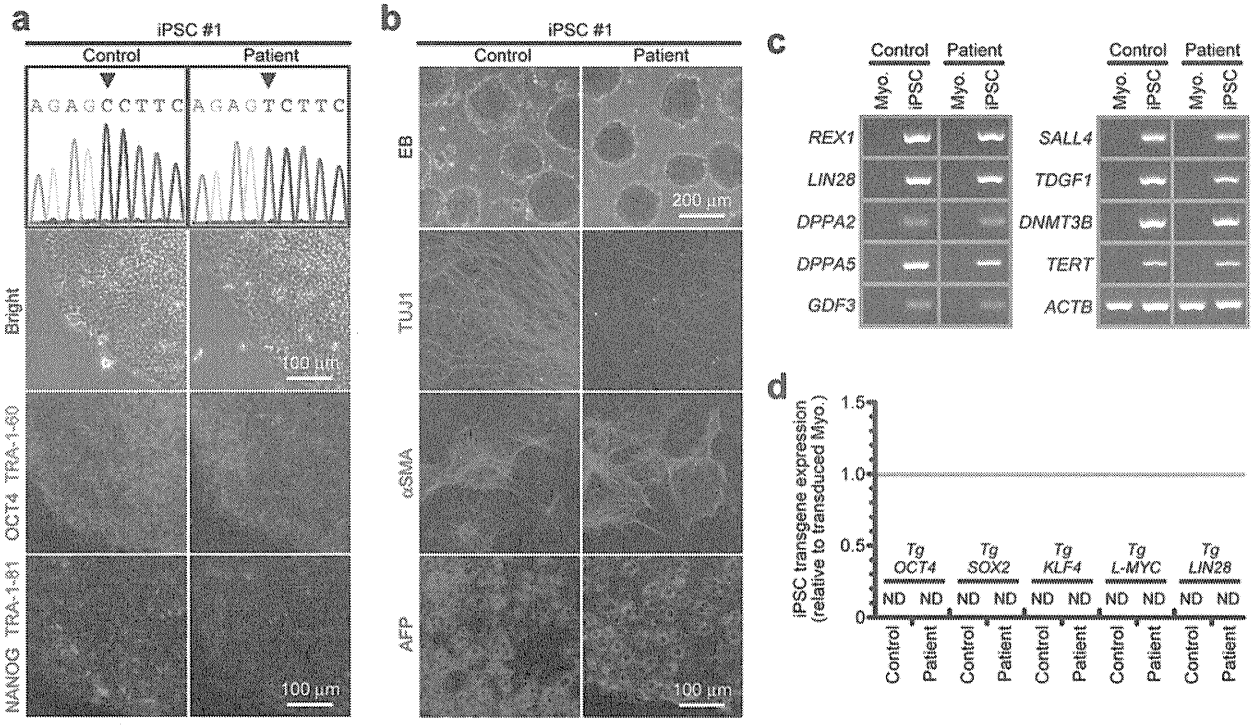

Fig. 3 Generation of disease-relevant iPSCs carrying all mutant mitochondrial $tRNA^{Trp}$. **a** Representative images of the established iPSC lines; OCT4 (red), NANOG (red), TRA-1-60 (green), TRA-1-81 (green). Arrowheads in electropherograms indicate m.5541C > T. **b** Representative images of the embryoid body (EB)-mediated *in vitro* spontaneous differentiation into three germ layers; TUJ1 (ectoderm, red), αSMA (mesoderm, red), AFP (endoderm, red). **c** Expression of other representative pluripotency genes in the established iPSC lines. **d** Silencing of transgenes expression in the established iPSC lines. Parental myoblasts after 7 days of transduction were also used as positive samples for both control and the patient. Expression level of each transgene was calculated using $\Delta\Delta C_T$-based relative quantification method by real-time PCR. Measurements were performed in triplicate. ND: Not Detected

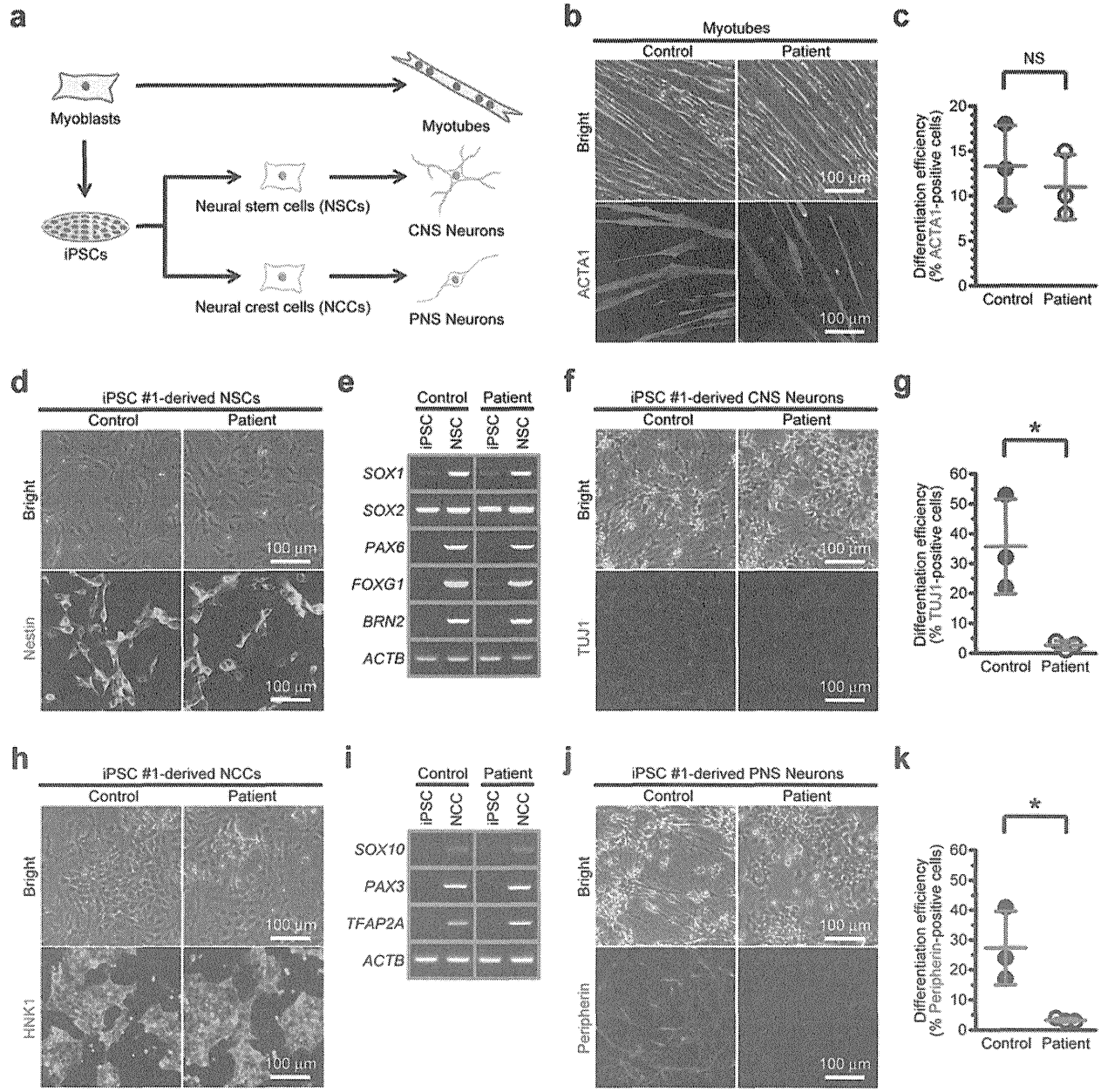

Fig. 4 Mutant mitochondrial $tRNA^{Trp}$ strongly impairs neuronal maturation, but does not affect skeletal muscle development. **a** Experimental design used to identify patient-specific disease phenotypes triggered by m.5541C > T. **b** Representative images of myotubes after 2 weeks of differentiation; ACTA1 (red). Cell nuclei were co-stained with Hoechst 33342 (blue). **c** Differentiation efficiency of myoblasts into myotubes. The number of ACTA1-positive myotubes was counted using a cytometer to estimate differentiation efficiency. Assays were performed using 3 experimental replicates for both control and the patient. Error bars indicate as the means with SD. Statistical significance was evaluated by unpaired, two-tailed *t*-test. NS: Not Significant. **d** Representative images of iPSC-derived NSCs; Nestin (green). **e** Expression of representative NSC marker genes in iPSC-derived NSCs. **f** Representative images of CNS neurons after 2 weeks of differentiation; TUJ1 (red). Cell nuclei were co-stained with Hoechst 33342 (blue). **g** Differentiation efficiency of NSCs into CNS neurons. The number of TUJ1-positive CNS neurons was counted using a cytometer to estimate differentiation efficiency. Assays were performed using 3 experimental replicates for both control and the patient. Error bars indicate as the means with SD. Statistical significance was evaluated by unpaired, two-tailed *t*-test. *: $P < 0.05$. **h** Representative images of iPSC-derived NCCs; HNK1 (green). **i** Expression of representative NCC marker genes in iPSC-derived NCCs. **j** Representative images of PNS neurons after 2 weeks of differentiation;
Peripherin (red). Cell nuclei were co-stained with Hoechst 33342 (blue). **k** Differentiation efficiency of NCCs into PNS neurons. The number of Peripherin-positive PNS neurons was counted using a cytometer to estimate differentiation efficiency. Assays were performed using 3 experimental replicates for both control and the patient. Error bars indicate as the means with SD. Statistical significance was evaluated by unpaired, two-tailed *t*-test. *: $P < 0.05$

harvested patient-derived myoblasts (1×10^5 cells/assay) were applied for measurement. A spectrophotometer equipped with thermostated unit (U-2010; Hitachi) was used, and a base line calibration was done before each measurement.

For CI activity measurement, cells were added into reaction buffer [pH 7.4; 50 mM Tris–HCl, 250 mM sucrose, 1 mM EDTA, 10 μM decylubiquinone, 50 μM NADH, 5 μg/mL antimycin A, 2 mM potassium cyanide] and were incubated at 37 °C. CI activity was monitored by time-dependent absorbance alterations.

For CII activity measurement, cells were added into reaction buffer [pH 7.4; 50 mM potassium phosphate, 20 mM succinate, 50 μM 2,6-dichlorophenolindophenol, 50 μM decylubiquinone, 5 μg/mL rotenone, 5 μg/mL antimycin A, 2 mM potassium cyanide] and were incubated at 37 °C. CII activity was monitored by time-dependent absorbance alterations.

For CIII activity measurement, cells were added into reaction buffer [pH 7.4; 50 mM Tris–HCl, 250 mM sucrose, 1 mM EDTA, 50 μM cytochrome *c*, 50 μM decylubiquinol (reduced form of decylubiquinone), 2 mM potassium cyanide] and were incubated at 37 °C. CIII activity was monitored by time-dependent absorbance alterations.

For CIV activity measurement, cells were added into reaction buffer [pH 7.4; 10 mM potassium phosphate, 25 μM ferrocytochrome *c* (reduced form of cytochrome *c*)] and were incubated at 37 °C. CIV activity was monitored by time-dependent absorbance alterations.

For citrate synthase (CS) activity measurement, cells were added into reaction buffer [pH 8.0; 125 mM Tris–HCl, 300 μM acetyl-CoA, 100 μM 5,5'-dithiobis (2-nitrobenzoic acid), 500 μM oxaloacetate] and were incubated at 37 °C. CS activity was monitored by time-dependent absorbance alterations.

Electrophoretic separation of mitochondrial proteins

Sodium dodecyl sulfate polyacrylamide gel electrophoresis (SDS-PAGE) [21] and blue native polyacrylamide gel electrophoresis (BN-PAGE) [22] were performed as described elsewhere with modifications, respectively: Cultured and harvested patient-derived myoblasts were resuspended in isolation buffer [pH 7.4; 210 mM mannitol, 70 mM sucrose, 1 mM EGTA, 5 mM HEPES] and were homogenated on ice. Cell lysates were centrifuged to isolate mitochondrial proteins. Obtained mitochondrial proteins were quantified by Bradford assay, and a calibration curve was created using several known concentrations of BSA.

For SDS-PAGE, isolated mitochondrial proteins (100 μg) were solubilized with 0.5 % SDS containing 50 mM dithiothreitol at 70 °C for 10 min. Electrophoresis was performed on 4 –12 % NuPAGE polyacrylamide gel (Invitrogen) at room temperature under 200 V constant.

For BN-PAGE, isolated mitochondrial proteins (100 μg) were solubilized with either 0.5 % *n*-dodecyl-β-d-maltoside (individual complexes detection) or 1 % digitonin (supercomplexes detection) on ice for 30 min. Insoluble proteins were removed by centrifugation. Electrophoresis was performed on 3 –12 % NativePAGE polyacrylamide gel (Invitrogen) at 4 °C under 150 V constant for 30 min, then resumed at 4 °C under 250 V constant.

Western blot for immunodetection of mitochondrial proteins

Electrophoresed gels were blotted onto polyvinylidene fluoride (PVDF) membranes using an iBlot transfer system (Invitrogen) according to the manufacturer's instructions. Blotted PVDF membranes were blocked at room temperature for 30 min. Primary antibody probing was performed at room temperature for 90 min. Secondary antibody probing was performed with chromogenic antibody detection kit (WesternBreeze; Invitrogen) according to the manufacturer's instructions. Primary antibodies used for SDS-PAGE were as follows: 0.5 μg/mL anti-porin (Molecular Probes), 2.5 μg/mL anti-MT-CO1 (Molecular Probes), 2.5 μg/mL anti-MT-CO2 (Molecular Probes), 2.5 μg/mL anti-COX4 (Molecular Probes), 2.5 μg/mL anti-COX5B (Molecular Probes). Primary antibodies used for BN-PAGE were as follows: 0.5 μg/mL anti-NDUFA9 for CI (Molecular Probes), 0.5 μg/mL anti-SDHA for CII (Molecular Probes), 0.5 μg/mL anti-UQCRC2 for CIII (Molecular Probes), 2.5 μg/mL anti-MT-CO1 for CIV (Molecular Probes), 0.5 μg/mL anti-ATP5B for CV (Molecular Probes).

Cytochemical staining

Patient-derived myoblasts were seeded onto 4-well culture slides and were maintained at 37 °C under humidified atmosphere of 5 % CO_2. After 3 days in culture, cytochemical staining was performed as follows:

For cytochemical COX staining, cells were stained with reaction buffer [pH 5.5; 100 mM sodium acetate, 0.1 % $MnCl_2$, 0.001 % H_2O_2, 10 mM diaminobenzidine] at 37 °C for 1 h, followed by subsequent incubation with 1 % $CuSO_4$ at 37 °C for 5 min. Cell nuclei were co-stained with hematoxylin. Stained cells were rinsed, fixed, and dehydrated according to standard histological protocol. Samples were sealed with cover glass and were observed under an optical microscope (BX50 System; Olympus).

For cytochemical SDH staining, cells were stained with reaction buffer [pH 7.4; 50 mM succinate, 1 mM nitrotetrazolium blue] at 37 °C for 1 h. Cell nuclei were co-stained with hematoxylin. Stained cells were rinsed, fixed, and dehydrated according to standard histological

protocol. Samples were sealed with cover glass and were observed under an optical microscope (BX50 System; Olympus).

Immunocytochemical detection of CIV structural subunits

Patient-derived myoblasts were seeded onto 4-well culture slides and were maintained at 37 °C under humidified atmosphere of 5 % CO_2. After 3 days in culture, cells were fixed, permeabilized, and blocked according to standard immunocytochemical protocol. Primary antibody probing was performed at room temperature for 2 h. Secondary antibody probing was performed with 2.5 μg/mL Alexa Fluor 568 (Molecular Probes) at room temperature for 1 h. Mitochondria were co-stained with 0.25 μg/mL MitoTracker Green (Molecular Probes). Stained cells were observed under a fluorescent microscope (IX71 System; Olympus). Primary antibodies used were as follows: 2.5 μg/mL anti-MT-CO1 (Molecular Probes), 2.5 μg/mL anti-COX4 (Molecular Probes).

Analysis of ATP level

Cultured and harvested patient-derived myoblasts (100 cells/assay) were applied for measurement. ATP amount was monitored with rLuciferase/Luciferin chemiluminescence-based ATP detection kit (Promega) according to the manufacturer's instructions. A chemiluminescent multi-well plate reader (Centro LB 960; Berthold Technologies) was used, and a calibration curve was created using several known concentrations of ATP.

Analysis of oxidative stress level and membrane potential level

Patient-derived myoblasts were seeded onto 96-well culture plate and were maintained at 37 °C under humidified atmosphere of 5 % CO_2. After 3 days in culture, cells were stained at 37 °C for 1 h. Stained cells were rinsed and were measured on a fluorescent multi-well plate reader (ARVO SX; Perkin Elmer); first at excitation/emission of 545/595 nm (red fluorescence) and then sequentially at excitation/emission of 485/535 nm (green fluorescence). Fluorescent dyes used were as follows: 0.25 μg/mL MitoTracker Green (Molecular Probes), 0.25 μg/mL MitoSOX Red (Molecular Probes), 0.25 μg/mL JC-1 (Molecular Probes).

Generation of patient-derived iPSCs with episomal vector

Patient-derived iPSCs were generated using episomal vectors as described previously [23] with modifications: Briefly, each 1 μg of episomal plasmid vectors (Plasmid #27077, #27078, #27080; Addgene) were electroporated into patient-derived myoblasts (5×10^5 cells) with an electroporator (Neon; Invitrogen). Transformed patient-derived myoblasts (1×10^5 cells) were reseeded onto mouse embryonic fibroblasts (MEF; ReproCELL) 4 days after electroporation. The next day, culture medium was replaced with primate ESC culture medium (ReproCELL) supplemented with 10 ng/mL bFGF (ReproCELL), 100 units/mL penicillin (Gibco), 100 μg/mL streptomycin (Gibco), and transformed patient-derived myoblasts were maintained at 37 °C under humidified atmosphere of 5 % CO_2. Emergent colonies with ESC-like morphology were manually picked up to establish patient-derived iPSCs, and these iPSCs were expanded either on MEF-seeded dishes in primate ESC culture medium or on Geltrex (Gibco)-coated dishes in mTeSR1 medium (STEMCELL Technologies) supplemented with 100 units/mL penicillin (Gibco), 100 μg/mL streptomycin (Gibco) for long-term maintenance.

Characterization of patient-derived iPSCs

Characterization of patient-derived iPSCs via detection of pluripotency markers was performed as follows: Briefly, cultured and harvested patient-derived iPSCs were transferred onto MEF-seeded 6-well culture plates and were maintained in primate ESC culture medium at 37 °C under humidified atmosphere of 5 % CO_2. After 3 days in culture, patient-derived iPSCs were characterized by immunocytochemical staining. Fluorophore-conjugated primary antibodies used were as follows: 5 μg/mL Cy3-conjugated anti-OCT4 (Millipore), 5 μg/mL Cy3-conjugated anti-NANOG (Millipore), 5 μg/mL AlexaFluor 488-conjugated anti-TRA-1-60 (Millipore), 5 μg/mL AlexaFluor 488-conjugated anti-TRA-1-81 (Millipore).

in vitro spontaneous differentiation of patient-derived iPSCs into EB-mediated three germ layers was performed as follows: Briefly, cultured and harvested patient-derived iPSCs were transferred onto ultra-low-adherent culture dishes (HydroCell; CellSeed) and were maintained in primate ESC culture medium without bFGF at 37 °C under humidified atmosphere of 5 % CO_2. After 7 days in floating culture, emergent EBs were transferred onto gelatin-coated 6-well culture plates and were maintained in primate ESC culture medium without bFGF at 37 °C under humidified atmosphere of 5 % CO_2. After 14 additional days in adherent culture, spontaneously differentiated cells were characterized by immunocytochemical staining. Primary antibodies used were as follows: 5 μg/mL anti-TUJ1 for ectoderm (Abcam), 5 μg/mL anti-αSMA for mesoderm (Abcam), 5 μg/mL anti-AFP for endoderm (Abcam). Secondary antibody used was 2.5 μg/mL Alexa Fluor 568 (Molecular Probes).

Directed differentiation of iPSCs into neural stem cells (NSCs)

Directed differentiation of patient-derived iPSCs into NSCs was performed according to a previous report

[24] with modifications: Briefly, patient-derived iPSCs were seeded onto Geltrex-coated dishes and were maintained in mTeSR1 medium at 37 °C under humidified atmosphere of 5 % CO_2. After 3 days in adherent culture, culture medium was switched to NSC induction medium [1:1 mixture of DMEM/F12 (Gibco) and Neurobasal medium (Gibco) supplemented with 1 × N2 (Gibco), 1 × B27 minus vitamin A (Gibco), 1 × GlutaMAX (Gibco), 100 units/mL penicillin (Gibco), 100 μg/mL streptomycin (Gibco), 10 μM SB431542 (Wako), 100 nM LDN193189 (Wako), 20 ng/mL EGF (Peprotech), 20 ng/mL bFGF (Peprotech)], and patient-derived iPSCs were maintained at 37 °C under humidified atmosphere of 5 % CO_2. Emergent NSCs were expanded in NSC induction medium and were characterized by immunocytochemical staining. Fluorophore-conjugated primary antibody used was 5 μg/mL AlexaFluor 488-conjugated anti-Nestin (Millipore).

Directed differentiation of iPSCs into neural crest cells (NCCs)

Directed differentiation of patient-derived iPSCs into NCCs was performed according to a previous report [25] with modifications: Briefly, patient-derived iPSCs were seeded onto Geltrex-coated dishes and were maintained in mTeSR1 medium at 37 °C under humidified atmosphere of 5 % CO_2. After 3 days in adherent culture, culture medium was switched to NCC induction medium [mTeSR1 medium (STEMCELL Technologies) supplemented with 100 units/mL penicillin (Gibco), 100 μg/mL streptomycin (Gibco), 2 μM (2'Z,3'E)-6-bromoindirubin-3'-oxime (Wako), 20 μM SB431542 (Wako)], and patient-derived iPSCs were maintained at 37 °C under humidified atmosphere of 5 % CO_2. Emergent NCCs were expanded in NCC induction medium and were characterized by immunocytochemical staining. Fluorophore-conjugated primary antibody used was 5 μg/mL FITC-conjugated anti-HNK1 (Miltenyi Biotec).

Terminal differentiation of NSCs and NCCs into neurons

Terminal differentiation of patient-derived NSCs and NCCs into neurons was performed as follows: Briefly, patient-derived NSCs and NCCs were seeded at high cell density onto Geltrex-coated 6-well culture plates and were maintained at 37 °C under humidified atmosphere of 5 % CO_2. After 3 days in culture, culture medium was switched to neuron induction medium [Neurobasal medium (Gibco) supplemented with 1 × N2 (Gibco), 1 × B27 minus vitamin A (Gibco), 1 × GlutaMAX (Gibco), 100 units/mL penicillin (Gibco), 100 μg/mL streptomycin (Gibco), 10 ng/mL BDNF (Peprotech), 10 ng/mL GDNF (Peprotech), 10 ng/mL NGF (Peprotech), 500 μM dbcAMP (Sigma), 200 μM ascorbic acid (Wako)], and patient-derived NSCs and NCCs were maintained at 37 °C under humidified atmosphere of 5 % CO_2 for more than 2 weeks. For immunocytochemical detection of emergent NSC-derived neurons, 5 μg/mL anti-TUJ1 (Abcam) and 2.5 μg/mL Alexa Fluor 568 (Molecular Probes) were used. For immunocytochemical detection of emergent NCC-derived neurons, 5 μg/mL PE-conjugated anti-Peripherin (Santa Cruz) was used.

Results

Molecular pathomechanisms of mutant mitochondrial $tRNA^{Trp}$

We found a patient who was clinically diagnosed as MELAS with multiple organ involvement including hypertrophic cardiomyopathy, acute pancreatitis, gastrointestinal malabsorption, renal tubular disturbance, and endocrine glucose intolerance (Fig. 1a-d). We identified a disease-causative mutation, m.5541C > T heteroplasmy in *MT-TW* gene, in this patient (Fig. 1e and Additional file 1: Table S1). Skeletal muscle tissues and the established myoblasts showed quite high mutant proportions (~100 %), whereas blood tissues showed relatively low mutant proportions (~50 %). The same m.5541C > T heteroplasmy was also observed in blood tissues from this patient's asymptomatic mother at quite low mutation levels (~10 %). The mutated position in the anticodon-stem of *MT-TW* gene was evolutionarily conserved through most parts of primates and typical eukaryotes (Fig. 1f). We also performed *in silico* calculation of mitochondrial $tRNA^{Trp}$ stability for both wild-type and m.5541C > T mutant (Additional file 1: Figure S1). Mutant mitochondrial $tRNA^{Trp}$ was destabilized by m.5541C > T and was probably existed more physicochemically stable but biochemically inappropriate conformation. Our findings suggest that m.5541C > T presumably induces defects in mitochondrial $tRNA^{Trp}$-associated translation machinery.

Although m.5541C > T was previously reported and predicted as "definitely pathogenic" [26], and our patient was the second case to show this mutation, the detailed molecular pathomechanisms of m.5541C > T —how this mutation influences mitochondrial pathophysiology, which is closely related to the variation and the severity of clinical symptoms in affected individuals— remain unclear. We comprehensively evaluated mitochondrial function using patient-derived myoblasts carrying quasi-homoplasmic m.5541C > T (*i.e.*, ~100 % mutant mtDNA exists within a cell). On mitochondrial respiratory chain complexes, severely decreased CIV activity and moderately decreased CI activity were both detected in the patient, whereas the other respiratory chain complexes showed within normal ranges (Fig. 2a,b). CIV holoenzyme and CIV-containing respiratory supramolecular architectures were also diminished in the patient, whereas

the other respiratory chain complexes showed almost normal levels with the exception of moderately decreased CI holoenzyme amount (Fig. 2c,d). Such CIV holoenzyme deficits in the patient were most likely because of decreased mRNA and protein expression levels of mtDNA-encoded CIV structural subunits (Fig. 2e-g). On mitochondrial physiology, widespread dysfunction such as decreased ATP level, increased oxidative stress level, and damaged membrane potential level were all observed in the patient (Fig. 2h-j). We also performed *in silico* prediction on mitochondrial tryptophan contents and their locations in each mtDNA-encoded CIV structural subunit (Additional file 1: Figure S2). Amino acid sequences in all mtDNA-encoded CIV structural subunits showed high homology between bovine and human, and bovine mitochondrial tryptophan residues were predominantly located in α-helix and β-sheet domains essential for the maintenance of CIV structural subunit conformations. Some human mitochondrial tryptophan residues in mtDNA-encoded CIV structural subunits were also located at the boundary between CIV structural subunits necessary for CIV holoenzyme assembly. Our results clearly indicate that m.5541C > T primarily induces the aberrant steady-state of mitochondrial respiratory chain complexes, followed by severely injured mitochondrial homeostasis.

Cell-type-specific disease phenotypes of MELAS using patient-derived iPSCs carrying all mutant mitochondrial $tRNA^{Trp}$

We next generated each 3 lines of integration-free disease-relevant iPSCs derived from myoblasts of both control and the patient carrying quasi-homoplasmic m.5541C > T as *in vitro* disease models. No apparent differences in embryonic stem cell (ESC)-like pluripotent characteristics were confirmed between iPSCs derived from control and the patient (Fig. 3 and Additional file 1: Figure S3). To elucidate patient-specific cellular disease phenotypes triggered by quasi-homoplasmic m.5541C > T, we used myotubes and iPSC-derived neurons of both control and the patient (Fig. 4a). In myogenic lineage, no significant differences in *in vitro* differentiation propensity into ACTA1-positive myotubes were observed between control and the patient (Fig. 4b,c). This phenomenon indicates that m.5541C > T seems not to affect skeletal muscle development in the patient regardless of serious mitochondrial dysfunction (see also Figs. 1d and 2). We differentiated patient-derived iPSCs into central nervous system (CNS) lineage. Efficient differentiation into nestin-positive NSCs (>95 % conversion) was observed in both control and the patient (Fig. 4d,e and Additional file 1: Figure S4a); however, the number of TUJ1-positive mature CNS neurons was markedly decreased only in the patient (Fig. 4f,g and Additional file 1: Figure S4b), and most parts of patient-derived differentiating NSCs finally died during long-term terminal differentiation (data not shown). We also differentiated patient-derived iPSCs into peripheral nervous system (PNS) lineage. A trend quite similar to CNS lineage, stable differentiation into HNK1-positive NCCs (>95 % conversion) was confirmed in both control and the patient (Fig. 4h,i and Additional file 1: Figure S4c); however, significant decrease of peripherin-positive mature PNS neurons was detected only in the patient (Fig. 4j,k and Additional file 1: Figure S4d), and patient-derived differentiating NCCs no longer survived during extended periods of neuronal maturation (data not shown). Several recent studies have demonstrated that mitochondria are gradually rejuvenated to an ESC-like "quiescent state" during cellular reprogramming [27–30]. Our results also suggest that stem/progenitor cells of both CNS and PNS lineages are minimally influenced by m.5541C > T, most likely because these cell types may possess a less active mitochondrial respiration state similar to ESCs and iPSCs. Therefore, we conclude that the molecular pathogenicity of m.5541C > T is strongly visible in terminally differentiated post-mitotic neurons, but not their stem/progenitor cells, which is probably associated with the degree of mitochondrial maturation during cellular lineage-commitment process.

Discussion

The molecular pathomechanisms of m.5541C > T can be summarized as follows: This mutation firstly loses the appropriate base pair interaction, from Watson-Crick to T-G mismatching, in the anticodon-stem of *MT-TW* gene and induces defects in mitochondrial $tRNA^{Trp}$-associated translation machinery most likely due to inadequate anticodon recognition of mitochondrial tryptophan by its altered conformation. Mutant mitochondrial $tRNA^{Trp}$ disturbs the synthesis of mtDNA-encoded respiratory chain complexes subunits; in this case, markedly decreased amounts of mtDNA-encoded CIV subunits predominantly inhibit CIV holoenzyme formation at each assembly process [31]. In fact, some patients carrying this mutation or other reported pathogenic mutations in the anticodon-stem of *MT-TW* gene also present severe COX deficiency [8, 26, 32]. Therefore, our findings clearly demonstrate why mutant mitochondrial $tRNA^{Trp}$ is able to cause severe COX deficiency as one of common clinical phenotypes. Induced mitochondrial respiratory dysfunction triggered by loss of CIV holoenzyme severely impairs mitochondrial biogenesis and bioenergetics such as decreased ATP level, increased oxidative stress level, and damaged membrane potential level. Increased oxidative stress level may promote the accumulation of oxidative damages to other mitochondrial enzymes, substrates, lipids, and mtDNA, all of which lead to premature cell senescence. Damaged membrane potential level may also

accelerate the leakage of cytochrome *c* molecules in mitochondrial electron transport system, which induces apoptotic cell death. Thus, m.5541C > T causes widespread mitochondrial dysfunction, which is closely related to cell-type-specific physiological impairment in various post-mitotic tissues and organs in this patient.

This case is consistent with MELAS with multiple organ involvement characterized by its various clinical symptoms; however, we did not find any typical abnormalities in patient-derived skeletal muscle tissues other than diffuse COX deficiency. Generally, 80-90 % of MELAS patients those carrying mutant mtDNAs (*e.g.*, m.3243A > G in *MT-TL1* gene) exhibit ragged-red-fibers and/or strongly SDH-reactive blood vessels in skeletal muscle tissues, which indicate morphological, numerical, and/or physiological abnormalities in mitochondria. These findings suggest that quasi-homoplasmic m.5541C > T may cause rare pathological signatures in skeletal muscle development, presumably because this patient exhibits no significant differences in *in vitro* differentiation propensity into terminally differentiated myotubes as compared with control regardless of serious mitochondrial dysfunction.

Recently, several groups have also reported iPSC-based disease models for other heteroplasmic mutant mtDNAs [33-37]. As the common perceptions, intracellular mutant mtDNA proportions must always be considered for actual *in vitro* recapitulation of mitochondrial diseases at each cellular fate-determining process such as reprogramming, self-renewal, or differentiation. From this viewpoint, we generated integration-free patient-derived iPSCs carrying ~100 % mutant mtDNA and used them as *in vitro* cellular disease models to investigate the definitive genotype-phenotype relationship. We also demonstrated that terminally differentiated iPSC-derived CNS and PNS neurons, but not their stem/progenitor cells, are strongly influenced by m.5541C>T, most likely because the molecular pathogenic severity of mutant mitochondrial $tRNA^{Trp}$ may be determined by the degree of physiological and morphological maturation in mitochondria. Although our presenting results do not completely elucidate the relationship between *in vitro* cellular disease phenotypes and *in vivo* clinical symptoms of this patient, our approach would be widely available for understanding *bona fide* molecular pathomechanisms and cellular pathophysiology of affected tissues and organs in patients carrying heteroplasmic mtDNA mutations, as well as for further drug discovery applications.

Conclusions

Throughout this study, we identified the "definite" molecular pathomechanisms of m.5541C>T and demonstrated cell-type-specific *in vitro* disease phenotypes triggered by mutant mitochondrial $tRNA^{Trp}$ using integration-free disease-relevant iPSCs derived from myoblasts of the patient. Our iPSC-based strategy therefore holds enormous promise for the development of evidence-based, personalized diagnostics and therapeutics to patients exhibiting various mitochondrial diseases.

Additional file

Additional file 1: Supplementary Figures and Tables. (DOC 4252 kb) **Figure S1.** Comparison of mitochondrial tRNATrp stability between wild-type and m.5541C > T mutant (related to Fig. 1). **Figure S2.** Protein modeling and amino acid sequences of each mtDNA-encoded CIV subunit (related to Fig. 2). **Figure S3.** Generation of disease-relevant iPSCs carrying all mutant mitochondrial tRNATrp (related to Fig. 3). **Figure S4.** Mutant mitochondrial tRNATrp strongly impairs neuronal maturation (related to Fig. 4). **Table S1.** mtDNA sequence variants in this patient. **Table S2.** Primer list. **Table S3.** TaqMan probe list.

Competing interests

The authors declare that they have no competing interests.

Authors' contribution

HH conceived the study, designed and performed experiments. AK, HK, and IN collected the patient's clinical data. HH and YG analyzed and interpreted data, wrote the manuscript. All authors read and approved the final manuscript.

Acknowledgements

We are grateful to the patient's family for participating in this study. We also thank Mayuko Kato, Junko Takei, Yumiko Ondo, Yasuha Ono, Saki Okabe, Miyuki Kanazawa, and Dr. Mutsumi Yokota (NCNP, Japan) for their assistances. We also appreciate Dr. Ikuya Nonaka (NCNP, Japan) for his critical comment on the manuscript.

This study was financially supported in part by Grant-in-Aid for Research on Intractable Diseases (Mitochondrial Disorders) from the Ministry of Health, Labour, and Welfare, Japan; by AMED-CREST from the Japan Agency for Medical Research and Development.

Author details

[1]Department of Mental Retardation and Birth Defect Research, National Institute of Neuroscience, National Center of Neurology and Psychiatry, Kodaira, Tokyo 187-8502, Japan. [2]AMED-CREST, Japan Agency for Medical Research and Development, Chiyoda-ku, Tokyo 100-0004, Japan. [3]Department of Child Neurology, National Center Hospital, National Center of Neurology and Psychiatry, Kodaira, Tokyo 187-8551, Japan. [4]Department of Neuromuscular Research, National Institute of Neuroscience, National Center of Neurology and Psychiatry, Kodaira, Tokyo 187-8502, Japan. [5]Medical Genome Center, National Center of Neurology and Psychiatry, Kodaira, Tokyo 187-8551, Japan.

Received: 21 July 2015 Accepted: 22 July 2015
Published online: 22 August 2015

References

1. Taylor RW, Turnbull DM (2005) Mitochondrial DNA mutations in human disease. Nat Rev Genet 6:389–402
2. Suzuki T, Nagao A, Suzuki T (2011) Human mitochondrial tRNAs: biogenesis, function, structural aspects, and diseases. Annu Rev Genet 45:299–329
3. Enriquez JA, Chomyn A, Attardi G (1995) MtDNA mutation in MERRF syndrome causes defective aminoacylation of $tRNA^{Lys}$ and premature translation termination. Nat Genet 10:47–55
4. Hao H, Moraes CT (1997) A disease-associated G5703A mutation in human mitochondrial DNA causes a conformational change and a marked decrease in steady-state levels of mitochondrial $tRNA^{Asn}$. Mol Cell Biol 17:6831–6837
5. Kaufmann P, Koga Y, Shanske S, Hirano M, DiMauro S, King MP (1996) Mitochondrial DNA and RNA processing in MELAS. Ann Neurol 40:172–180